AJBAR Vol. 4(6), December 2025: 43-57, ISSN: 2811-2881

Arid Zone Journal of Basic and Applied Research

Faculty of Science, Kashim Ibrahim University Maiduguri, Nigeria

Journal homepage: https://www.azjournalbar.com

Research Article

Synthesis, Structural Characterization, and Antioxidant Properties of Benzohydroxamic Acid-Derived Metal Complexes

Munirat S. Bute[a], Grema A. Mala[a], Hassan B. Yesufu[b], Hauwa A. Zarma[c], Malik A. Yurari[d], and Ibrahim Waziri[a*]

[a]Department of Pure and Applied Chemistry, University of Maiduguri, Maiduguri, Nigeria
[b]Department of Pharmaceutical Chemistry, University of Maiduguri, P.M.B. 1069, Maiduguri, Nigeria
[c]Department of Nutrition and Dietetics, University of Maiduguri, P.M.B. 1069, Maiduguri, Nigeria.
Department of Chemistry, Yobe State University, Damaturu, Nigeria

*Corresponding author's Email: waziriibrahim@unimaid.edu.ng, doi.org/10.55639/607.02010080

ARTICLE INFO:

Keywords:
Benzohydroxamic acid,
Transition metals,
Oxidative stress,
DPPH
radical scavenging,

ABSTRACT

In this study, a benzohydroxamic acid ligand (HL) was synthesized via the reaction of methyl-4-amino-2-methoxybenzoate with hydroxylamine sulphate. The ligand was subsequently complexed with Mn(II), Co(II), Ni(II), and Cu(II) ions using their respective salts in a 1:2 metal-to-ligand molar ratio to afford the corresponding complexes (C1–C4), respectively. The ligand and its complexes were characterized using infrared spectroscopy, UV–Visible spectroscopy, and elemental analysis. IR spectral data confirmed that HL acts as a bidentate, monoanionic ligand, coordinating through the oxygen atoms of the hydroxyl (–OH) and carbonyl (C=O) groups to form a five-membered chelate ring around the metal centre. The antioxidant potential of the ligand and its metal complexes was assessed *in vitro* using the DPPH free radical scavenging assay at concentrations ranging from 100 to 500 µg/mL. All tested samples exhibited concentration-dependent radical scavenging activity; however, the free ligand (HL) demonstrated higher antioxidant activity than its metal complexes across all concentrations, except Co(II) complex (C2), which outperformed the ligand. The IC_{50} values for the ligand and the complexes (C1-C4) were found to be 155.3, 403.1, 75.7, 601.9, and 440.7 µg/mL. Nonetheless, neither the ligand nor the complexes outperformed the standard antioxidant, ascorbic acid, which showed consistently superior activity (IC_{50} = 66.2 µg/mL). In general, the results highlight the antioxidant properties of the synthesized benzohydroxamic acid ligand and its metal complexes, supporting the relevance of hydroxamic acid derivatives as bioactive agents and warranting further investigation into their pharmacological potential.

Corresponding author: Ibrahim Waziri **Email:** waziriibrahim@unimaid.edu.ng
Department of Pure and Applied Chemistry, University of Maiduguri, Maiduguri, Nigeria

INTRODUCTION

Hydroxamic acids constitute an important class of organic compounds distinguished by the presence of the –CONHOH functional group (Figure 1), which imparts unique chelating and biological properties (Saleem *et al.,* 2020; Syed *et al.,* 2020). They are widely recognized for their strong metal-binding ability, enabling them to form stable complexes with a variety of transition metal ions through oxygen donor sites (Hassan *et al.,* 2018; Korkmaz & Özdemir, 2022). Owing to this versatile coordination behaviour, hydroxamic acids and their metal complexes have attracted sustained research interest across medicinal, analytical, and coordination chemistry (Ali & Abedullah, 2023; Citarella *et al.,* 2021). Beyond their well-established application as enzyme inhibitors, antitumor and antimicrobial agents, increasing attention has been directed toward exploring their antioxidant properties, due to the role of oxidative stress in the pathogenesis of numerous diseases (Aneja *et al.,* 2020; Keth *et al.,* 2020; Sow *et al.,* 2023).

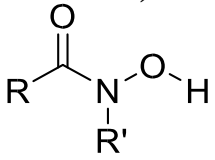

Figure 1: Hydroxamic acid general structure: R and R^1 are organic residues

Oxidative stress resulting from excessive free-radical generation contributes to cellular damage and has been linked to chronic disorders such as cancer, diabetes, cardiovascular and neurodegenerative diseases (Pooja *et al.*, 2025; Reddy, 2023; Sadiq, 2023). Although synthetic antioxidants exist, their long-term safety has been questioned, thereby necessitating the search for safer and more effective alternatives. Metal complexes of bioactive ligands have emerged as promising scaffolds for enhancing pharmacological properties, as metal coordination can modulate ligand redox behaviour, lipophilicity, and biological activity (Azimi *et al.,* 2025; Gambino & Otero, 2023; Kothawade & Shende, 2024; Naeem *et al.,* 2025). However, reports on the antioxidant potential of hydroxamic acid-derived metal complexes remain limited compared to other ligand systems such as Schiff bases, hydrazones, and phenolic compounds. There is a lack of systematic studies examining how coordination to different transition metals influences the antioxidant efficiency of hydroxamic acids, in the last three years (2022-2025).

To address this gap, the present study focuses on the synthesis, characterization, and antioxidant evaluation of a benzohydroxamic acid ligand and its Mn, Co, Ni, and Cu complexes. The ligand was synthesized from methyl-4-amino-2-methoxybenzoate and subsequently coordinated to selected transition metals to assess changes in structural and functional properties following complexation. Spectroscopic and physiochemical characterization was carried out using infrared and UV–Visible spectroscopy, alongside elemental analysis, to confirm ligand formation and coordination modes. The antioxidant activity of the ligand and metal complexes **were** assessed using the DPPH radical-scavenging assay.

Findings from this study contributes to the growing body of knowledge on hydroxamic acid-based metal complexes as potential therapeutic antioxidants and provide a platform for future mechanistic and biological investigations.

EXPERIMENTAL

Chemicals and Reagents

All chemicals and solvents used in this study were of analytical grade and were used without further purification unless otherwise stated. Hydroxylamine sulphate, sodium hydroxide, methyl-4-amino-2-methoxybenzoate, and sulfuric acid were employed as starting materials for the synthesis of the benzohydroxamic acid ligand. Manganese, cobalt, nickel, and copper acetates were used as the metal sources for the preparation of the corresponding metal complexes. All reagents were procured from Sigma-Aldrich and Merck and were stored in tightly sealed containers under appropriate laboratory conditions to prevent contamination and moisture uptake.

Synthesis of the hydroxamic acid ligand: 4-amino-*N*-hydroxy-2-methoxybenzamide (HL)

The ligand was synthesized following the literature procedure reported by (Mohammed, 2019), with slight modifications. Hydroxylamine sulphate (6.11 g, 37.0 mmol, 1 eq) was added to a stirring mixture of crushed

ice (30 g), sodium hydroxide (7.41 g, 185 mmol, 5 eq) in 30 mL of distilled water, and sodium sulphate (0.58 g, 4.1 mmol, 0.11 eq). Subsequently, methyl-4-amino-2-methoxybenzoate (6.70 g, 37.0 mmol, 1 eq) was added, and the reaction mixture was stirred at 45 °C for 24 hours. After completion, the solution was allowed to cool to room temperature, and the pH was adjusted to 6 using dilute sulfuric acid to induce precipitation. The solid product formed was collected by suction filtration, washed with cold distilled water, and recrystallized from hot water to obtain the pure ligand. The synthetic pathway is illustrated in **Scheme 1**.

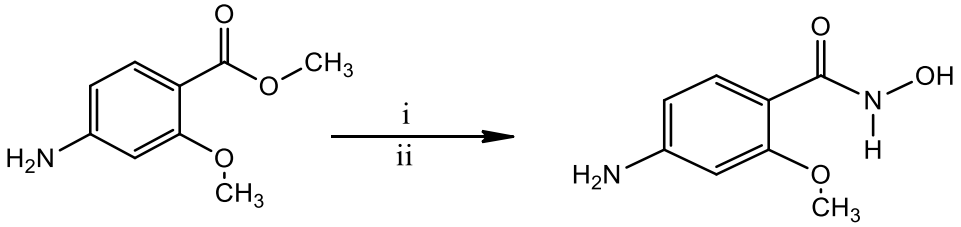

Scheme 1: Reaction pathway for the synthesis of the ligand (**HL);** i = $NH_2OH.H_2SO_4$, NaOH, Na_2SO_4, Ice, ii = 45 °C/24 h.

Grey powder, yield: 69 %, m.p.: 148 °C; UV-Vis (DMSO, 10^{-3} M) λ_{max} (nm): 245 ($\pi \rightarrow \pi^*$), 320 ($n \rightarrow \pi^*$); $FTIR_{ATR}$: U(cm^{-1}): 3300 (N-H), 3100 (O-H), 1670 (C=O), 1540 (C-N), 1270 (C-O), 1020 (N-O): Elemental composition (CHN): Calculated for $C_8H_{10}N_2O_3$ = C, 52.74; H, 5.53; N, 15.38; Experimentally obtained = C, 52.73; H, 5.50; N, 15.35

General Procedure for the Synthesis of Metal Complexes (C1–C4)

The metal complexes were synthesized by reacting the ligand (HL) with the respective metal acetates in a 2:1 ligand-to-metal molar ratio (Fugu *et al.*, 2021). A solution of HL (0.182 g, 1.0 mmol, 2 eq) in 10 mL of methanol was prepared in a separate flask. To this, a methanolic solution (10 mL) of each metal acetate salt: $Mn(OAc)_2$ (0.09 g, 0.5 mmol), $Co(OAc)_2 \cdot 4H_2O$ (0.13 g, 0.5 mmol), $Ni(OAc)_2 \cdot 4H_2O$ (0.12 g, 0.5 mmol), and $Cu(OAc)_2$ (0.09 g, 0.5 mmol), was added in separate reaction flasks. The reaction mixtures were stirred at room temperature for 6 hours. The resulting precipitates were collected by filtration, washed thoroughly with cold methanol and diethyl ether, and air-dried. In cases where no solid formed, the reaction mixtures were concentrated under reduced pressure to obtain the complexes (C1-C4), respectively. The synthesized complexes were then subjected to physicochemical and spectroscopic analyses for structural confirmation. The synthetic pathway is illustrated in **Scheme 2.**

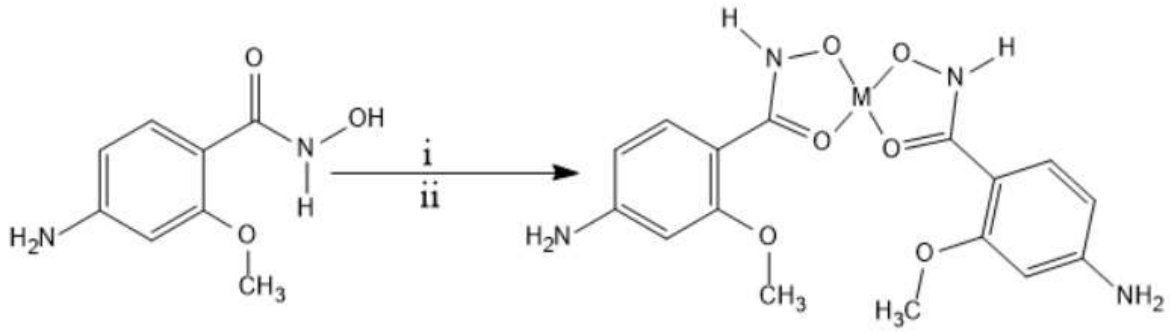

Scheme 2: Reaction pathway for the synthesis of the metal complexes (**C1-C4)**; i = $M(OAc)_2.nH_2O/CH_3OH$. ii = RT/6 hours; M = Mn, Co, Ni or Cu, n = 0 or 4

Bis-4-amino-*N*-hydroxy-2-methoxybenzamide manganese (C1)

Dark brown powder, yield: 63 %, m.p : 255 °C ; UV-Vis (DMSO, 10^{-3} M) λ_{max} (nm): 220 ($\pi \rightarrow \pi^*$), 300 ($n \rightarrow \pi^*$), 500 (LMCT); $FTIR_{ATR}$: υ(cm^{-1}): 1660 (C=O), 1540 (C-N), 120 (C-O), 1050 (N-O), 520 (Mn-O); Elemental composition (CHN): Calculated for $C_{16}H_{18}N_4MnO_6$ = C, 46.05; H, 4.35; N, 13.43; Experimentally obtained: C, 46.03; H, 4.33; N, 13.41

Bis-4-amino-*N*-hydroxy-2-methoxybenzamide cobalt (C2)

Black powder; yield: 66 %; m.p : 235 ºC ; UV-visible (DMSO, 10^{-3} M) λ_{max} (nm): 230 ($\pi\rightarrow\pi^*$), 300 ($n\rightarrow\pi^*$), 500 (LMCT); $FTIR_{ATR}$: υ(cm $^{-1}$): 1650 (C=O), 1560 (C-N), 1230 (C-O), 1030 (N-O), 560 Co-O); Elemental composition (CHN): Calculated for $C_{16}CoH_{18}N_4O_6$ = C, 45.62; H, 4.31; N, 13.30; Experimentally obtained: C, 45.63; H, 4.33; N, 13.31

Bis-4-amino-*N*-hydroxy-2-methoxybenzamide nickel (C3)

Dark brown powder; yield: 73 %; m.p : 248 ˚C ; UV-visible (DMSO, 10^{-3} M) λ_{max} (nm): 215 ($\pi\rightarrow\pi^*$), 315($n\rightarrow\pi^*$), 480 (LMCT); $FTIR_{ATR}$: υ(cm $^{-1}$): 1655 (C=O), 1545 (C-N), 1260 (C-O), 1040 (N-O), 425 (Ni-O); Elemental composition (CHN): Calculated for $C_{16}H_{18}N_4NiO_6$; C, 45.64; H, 4.31; N, 13.43; Experimentally obtained: C, 45.66; H, 4.32; N, 13.33

Bis-4-amino-*N*-hydroxy-2-methoxybenzamide copper (C4)

Black powder; yield: 74 %; m.p: 250 ºC ; UV-visible (DMSO, 10^{-3} M) λ_{max} (nm): 260 ($\pi\rightarrow\pi^*$), 310 ($n\rightarrow\pi^*$), 405 (LMCT); $FTIR_{ATR}$: υ(cm $^{-1}$): 1640 (C=O), 1550 (C-N), 1240 (C-O), 1060 (N-O), 530 (Cu-O); Elemental composition (CHN): Calculated for $C_{16}CuH_{18}N_4O_6$; C, 45.12; H, 4.26; N, 13.16; Experimentally obtained: C, 45.10; H, 4.23; N, 13.14

Measurements and Instrumentation

All spectroscopic and analytical measurements were performed using standard instrumentation. The FT-IR spectra of the ligand and its complexes were recorded in the solid state using a Bruker Tensor 27 FT-IR spectrometer and a PerkinElmer BX FT-IR spectrometer over the range 4000–400 cm^{-1}. Elemental (CHN) analysis was conducted using a Vario EL III Elementar microanalyzer to determine the percentage composition of carbon, hydrogen, and nitrogen. UV–Visible spectra were obtained on a PerkinElmer UV–Vis spectrophotometer in the wavelength range of 200–800 nm at room temperature, using 10^{-3} M solutions of the samples prepared in DMSO.

Antioxidant Activity

The antioxidant activity of the free ligand (HL) and its metal complexes (C1–C4) was assessed *in vitro* using the DPPH (2,2-diphenyl-1-picrylhydrazyl) radical scavenging assay, following the procedure reported by (Waziri *et al.,* 2023). A 3 mM DPPH stock solution was prepared in ethanol. Subsequently, 1 mL of the DPPH solution was mixed with 1 mL of the test sample solutions of the ligand and complexes at different concentrations (100–500 µg/mL). The reaction mixtures were then incubated in the dark at room temperature for 30 minutes to prevent photodegradation of the DPPH radical. The absorbance of each solution was recorded at 517 nm using a UV–Vis spectrophotometer, and all measurements were carried out in triplicate. The percentage radical scavenging activity was calculated using Equation presented below. Ascorbic acid served as the standard antioxidant (positive control), and IC_{50} values were determined following standard procedures.

$$\%SC = \frac{Ac-As}{Ac} \times 100$$

Where %SC = percentage scavenging, Ac = absorbance of the DPPH in methanol, and As = absorbance of the tested compounds with DPPH in methanol.

RESULTS AND DISCUSSION

Synthesis and Physical Properties

The synthetic pathways for the ligand (HL) and its metal complexes (C1-C4) are presented in Schemes 1 and 2. The ligand and its complexes were obtained in moderate yields of 63–74% as non-hygroscopic, air- and photostable solid powders. The complexes exhibited distinct colours, which is characteristic of transition metal complexes and arises from d–d electronic transitions (Waziri *et al.,* 2023).

The ligand melted at 148 °C, whereas the complexes showed higher melting points within the range of 235–250 °C. The sharp and well-defined melting points confirm the purity of the synthesized compounds, consistent with observations by (Hassan *et al.,* 2018). The higher melting points of the complexes relative to the free ligand indicate the formation of new coordination compounds with enhanced thermal stability and modified physicochemical properties upon metal chelation (Gani *et al.,* 2021).

Molar conductance measurements of 10^{-3} M methanolic solutions of the ligand and complexes were found to be low, ranging from 0.85 to 1.0 S cm^2 mol^{-1}, suggesting that the

complexes are weak or non-electrolytes in solution (Bagul *et al.,* 2023).

The solubility profiles of HL and its metal complexes were evaluated in solvents of varying polarity, namely distilled water, methanol, ethanol, diethyl ether, ethyl acetate, n-hexane, and benzene under both hot and cold conditions. The compounds were soluble or sparingly soluble in methanol and ethanol, but insoluble or only slightly soluble in non-polar and less polar solvents. This behaviour indicates the predominantly polar nature of the synthesized ligand and its complexes (de Araújo Queirós, 2018). To confirm the formation and coordination behaviour of the metal complexes, the ligand and its derivatives were further subjected to spectroscopic characterization, as described in the subsequent sections.

Spectroscopic Characterization

FTIR Spectral Study

The FTIR spectral study of the ligand and its complexes were performed in solid state using ATR method at a wavelength range of 4000-400 cm^{-1}, and summary of the spectral data are presented in Table 1. The spectrum of the benzohydroxamic acid ligand (HL) displays the characteristic hydroxamate features: a broad H-bonded ν(N–OH)/ν(O–H) envelope in the 3300–3100 cm^{-1} region, a strong amide ν(C=O) at 1670 cm^{-1}, amide/ν(C–N) at 1540 cm^{-1}, the C–O band at ~1270 cm^{-1}, the ν(N–O) of the –CONHOH group at 1020 cm^{-1} (Mohammed, 2019).

In all four complexes C1–C4, the broad ν(N–OH)/ν(O–H) band disappears, evidencing deprotonation and formation of the hydroxamate anion. Concomitantly, ν(C=O) shifts to lower wavenumber by ca. 20–40 cm^{-1} relative to HL, whereas amide/ν(C–N) shows a small upshift (≈ +5–20 cm^{-1}); together these trends indicate enhanced –CONO– delocalization on chelation. The ν(N–O) band also shifts (typically 10–30 cm^{-1} to lower frequency), consistent with participation of the N–O oxygen in binding. New absorptions appear in the far-IR attributable to ν(M–O), typically ~520–560 cm^{-1} (C=O–O→M) and (N–O→M), confirming O,O′-bidentate coordination. Small parallel movements in Ar–O/Ar–O–CH_3 bands (≤10 cm^{-1}) reflect the electronic effect of metal binding (He, 2019).

Across the series, the intensity and position of ν(M–O) suggest the expected increase in M–O bond stiffness, generally Cu ≳ Ni> Co > Mn, which correlates with the magnitude of the downshift in ν(C=O). The absence of carboxylate $\nu(COO)_{as}$ and $\nu(COO)_{sy}$ pairs from acetate indicates complete substitution of acetate by HL under the 2:1 (L:M) conditions. The bar chart (Figure 1) shows a systematic increase in both M–O stretching frequencies from Mn through Co and Ni to Cu, demonstrating enhanced metal–oxygen bond strength across the series. This trend correlates with increasing ligand field strength and metal–oxygen bond stiffness, confirming stronger coordination interactions for the later transition metals.

Table 1: FTIR bands (cm^{-1}) of HL and complexes C1–C4, showing diagnostic shifts confirming O,O′-bidentate coordination.

Assignment	HL (cm^{-1})	C1	C2	C3	C4	Diagnostic change
ν(N–OH)/ν(O–H)	3300–3100	—	—	—	—	Deprotonation
ν(C=O) (amide)	1670	1660	1650	1655	1640	Weakened C=O
ν(C–N)/amide	1540	1545	1560	1545	1550	More C=N character
ν(N–O)	1020	1050	1030	1040	1060	Delocalization
Ar–O / Ar–O–CH_3	1270	1230	1250	1260	1240	Electronic effect
ν(M–O)	—	520	560	525	530	Chelation confirmed

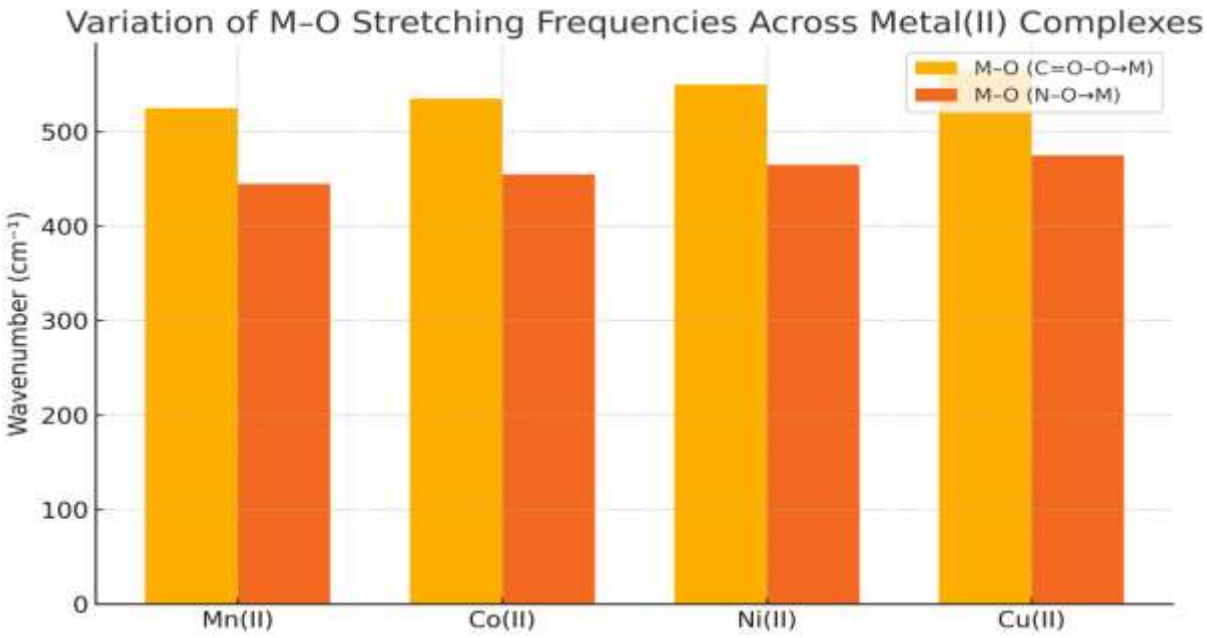

Figure 1: Clustered bar chart showing the M–O stretching frequencies for complexes C1–C4. The increasing ν(M–O) values from Mn to Cu reflect stronger metal–oxygen bonding across the series and support O,O′-bidentate coordination of the hydroxamate ligand in all complexes.

UV-Vis spectral study

The electronic behaviour of the ligand and its complexes was investigated using UV-Vis spectroscopy using a sample concentration of 10^{-3} M in dimethyl sulfoxide at a wavelength range of 200-800 nm. The summary of the spectral data and their respective band assignment are given in Table 2. The ligand HL shows two ligand-centred (Gulcin & Alwasel) bands at 245 nm and 320 nm, assigned to π→π* (anisyl/aromatic) and n→π* (hydroxamate C=O) transitions, respectively (Kumar *et al.*, 2024).

Upon coordination to Mn, Co, Ni and Cu (C1–C4), the LC transitions are perturbed and generally shift to higher energy (hypsochromic), consistent with deprotonation and O,O′-chelation that reduce lone-pair availability and slightly decrease effective conjugation in the ligand framework. Each complex also displays a new, broad absorption in the visible region that were assign to ligand-to-metal charge transfer (LMCT) from the O-donor to the metal centre (d–d bands are weak/obscured under these conditions) (Hao, 2020).

A clear trend is observed in the LMCT position: Mn ~500 nm → Co ~480 nm → Ni ~430 nm → Cu ~405 nm, i.e., a progressive blue shift across the series, indicating increasing M–O bond strength/acceptor ability for the later divalent ions. This electronic trend mirrors the FTIR evidence (larger ν(C=O) downshifts and stronger ν(M–O) for Ni/Cu), providing a coherent picture of stronger metal–oxygen interactions along the series. The LMCT energy trend (Mn(II) < Co < Ni < Cu reveals a systematic increase in charge-transfer efficiency towards the later transition metals, consistent with stronger M–O interactions and higher ligand-to-metal electron transfer capability across the series (Figure 2) (Howsaui *et al.*, 2021).

Table 2: Summary of UV–Vis absorption bands (λ_{max}, nm) for the ligand (HL) and its complexes (C1–C4

Compound	λ_{max} (nm)	Assignment
HL	245	π→π* (aryl/anisyl)
	320	n→π* (C=O, hydroxamate)
C1	220	π→π* (LC, blue-shifted)
	300	n→π* (LC, blue-shifted)
	500	LMCT (O→Mn^{2+})
C2	230	π→π* (LC, blue-shifted)
	300	n→π* (LC, blue-shifted)
	480	LMCT (O→Co^{2+})
C3	215	π→π* (LC, blue-shifted)
	280	n→π* (LC, blue-shifted)
	430	LMCT (O→Ni^{2+})
C4	260	π→π* (LC; intensity high; slightly red vs C1–C3 due to overlap/perturbation)
	310	n→π* (LC, blue-shifted vs HL)
	405	LMCT (O→Cu^{2+})

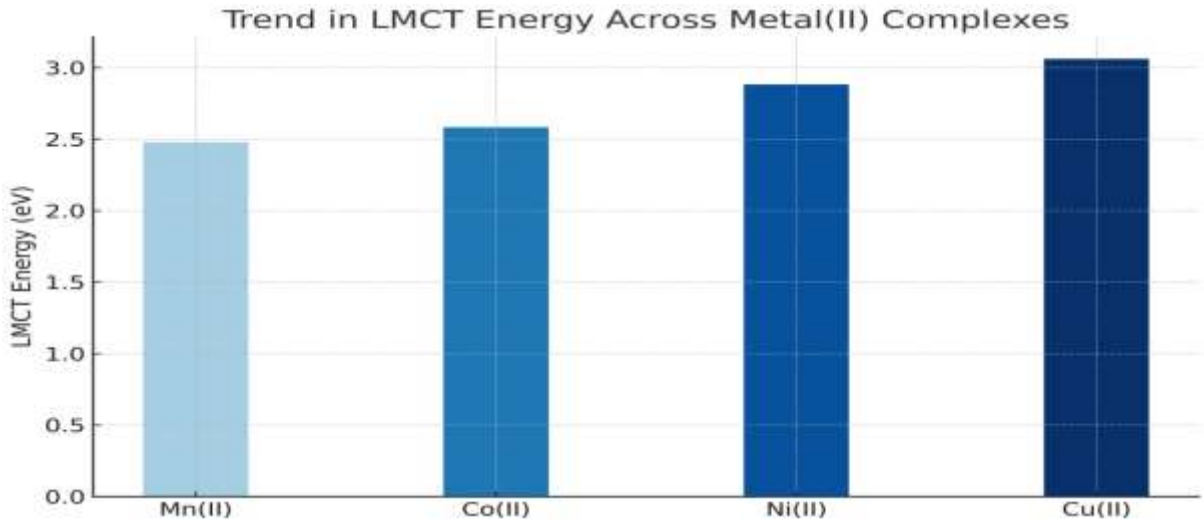

Figure 2: Bar chart showing the variation in LMCT transition energy across the Mn, Co, Ni, and Cu hydroxamate complexes. The progressive increase in LMCT energy from Mn to Cu indicates enhanced metal–oxygen charge-transfer interactions and stronger M–O bonding across the series.

Elemental Analysis (CHN)

The elemental (CHN) analytical data for the ligand (HL) and its metal complexes (C1–C4) showed excellent agreement between the experimentally found and theoretically calculated values, thus confirming the expected molecular compositions and high purity of the synthesized compounds. The calculated and found values for carbon, hydrogen, and nitrogen closely align for all compounds, with only minimal variations observed. This consistency strongly supports the successful formation of the hydroxamic acid ligand and its corresponding Mn, Co, Ni, and Cu complexes (C1-C4), in the proposed stoichiometric ratio. The close overlap of the calculated and found curves across all samples indicates negligible deviation, confirming the homogeneity and analytical correctness of the synthesized materials. To quantify this accuracy, the deviation plot in Figure 3 reveals that the differences between theoretical and experimental values for C, H, and N fall within an acceptable analytical threshold range of ±0.10%, which is well within the permissible margin for high-purity coordination compounds.

Collectively, these results validate the successful synthesis, compositional integrity, and purity of both the ligand and its metal complexes. The strong agreement between calculated and found elemental values provides foundational evidence supporting the proposed formulations and reinforces the reliability of subsequent spectral and analytical interpretations.

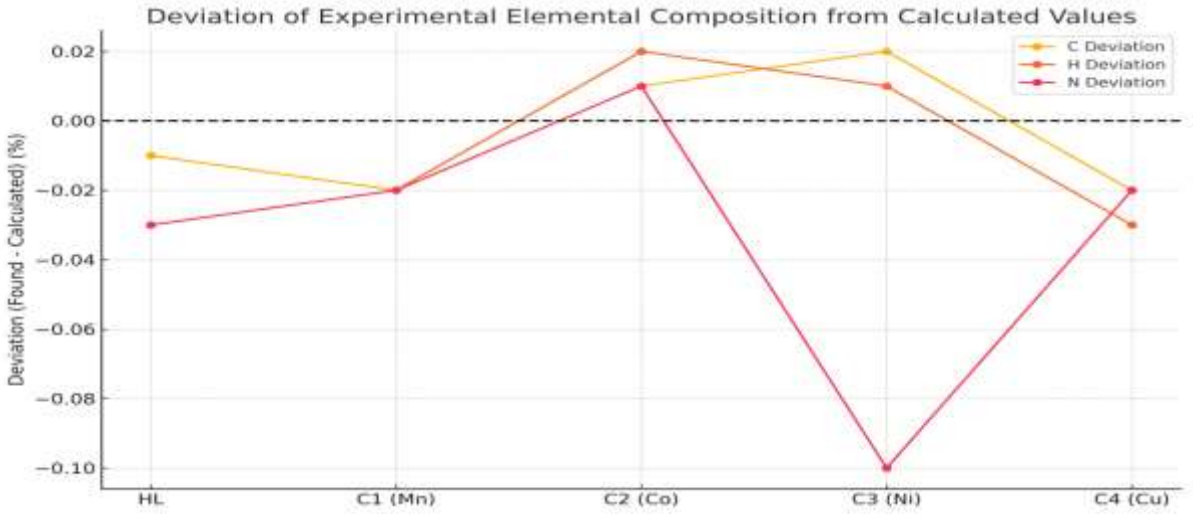

Figure 3: Deviation plot illustrating the percentage differences between calculated and experimental element composition values, all within ±0.10%, confirming excellent analytical agreement and high sample purity.

Proposed Structures

The structural formulation of the hydroxamic acid metal complexes illustrated in Scheme 2, which given in Figure 4 below is supported by the combined spectroscopic, analytical, and physicochemical data. The ligand (HL) functions as a bidentate monoanionic chelator, coordinating through the carbonyl (C=O) and deprotonated hydroxyl (O–H) oxygen atoms of the –CONHOH group to form a stable five-membered chelate ring. This coordination mode is evidenced by the downward shift of ν(C=O), disappearance/shift of ν(O–H), and the appearance of ν(M–O) bands in the IR spectra. Close agreement between the experimental and theoretical CHN values confirms the proposed 1:2 metal-to-ligand stoichiometry, while low molar conductance values support the formation of neutral $[M(L)_2]$ complexes. Higher melting points relative to the free ligand further indicate enhanced thermal stability upon coordination. Electronic spectra provided insight into the metal ion geometries: Mn, Co, and Ni complexes displayed weak d–d transitions consistent with distorted/perfect square plant tetrahedral geometries. LMCT bands and shifts in ligand-cantered transitions confirmed electronic perturbation due to coordination (Healy *et al.*, 2020; Rahban*et al.*, 2022)
.

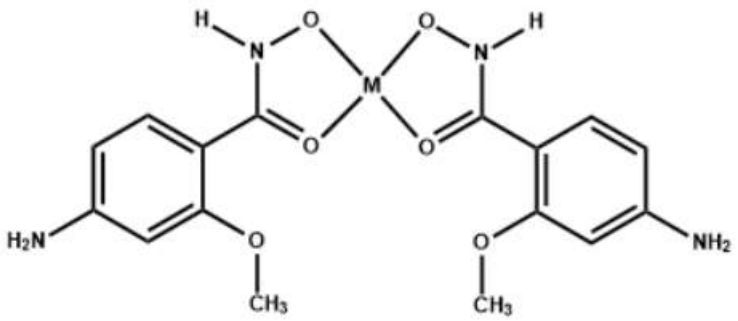

Figure 4: Proposed Structure for the Metal Complexes: M = Mn, Co, Ni, or Cu for C1-C4, respectively: A square planar geometry for C3 and C4, and tetrahedral geometry for C1 and C2.

Antioxidant Study

Having successfully confirmed the formation of the ligand and it complexes as detailed in the characterization section above. The ligand and its metal complexes were evaluated as a potential antioxidant agent using DPPH radical scavenging method at a sample concentration of (100–500 µg/mL) in comparison to ascorbic acid (control). The results obtained are presented in (Figures: 5-7), in form radical scavenging profile, activity index, and IC_{50} values, respectively. The DPPH scavenging profiles (Figure 5) show that the standard (AA) consistently outperforms all samples at every concentration, as expected. Among the test compounds, HL maintains relatively high activity (60–77%) across the series, whereas the complexes exhibit divergent behaviours: C2 (Co complex) performs best among the metal derivatives and becomes moderately active at low–mid concentrations, C4 (Cu) shows a monotonic increase with dose, C1 (Mn) improves sharply between 100–200 µg/mL then plateaus, and C3 (Ni) declines strongly with increasing concentration. Figure 6 compares the activity index of the ligand and its metal complexes relative to ascorbic acid (AA). The plot reveals that C2 (Co^{2+} complex) exhibited the highest activity index (87.4%), showing activity closest to the standard antioxidant, while the free ligand (HL) retained moderate radical scavenging potential (42.6%). In contrast, the Mn, Cu, and Ni complexes demonstrated considerably lower activity (16.4–11.0%), indicating that metal coordination generally diminished the antioxidant efficiency of the ligand, except in the case of Co^{2+}, where partial redox synergy enhanced DPPH reduction capability. The IC_{50} comparison plot (Figure 7) further highlights the influence of metal coordination on antioxidant potency. The Co complex (C2) exhibited the lowest IC_{50} among the synthesized complexes, closely approaching the standard ascorbic acid (AA), while the free ligand (HL) showed moderate activity. The Mn (C1) and Cu (C4) complexes displayed weaker but comparable effects, and the Ni complex (C3) recorded the highest IC_{50}, indicating the least scavenging efficiency. This trend reinforces the mechanistic SAR interpretation that Co, through favourable LMCT and Co/Co(III) redox cycling, enhances ET-mediated antioxidant activity, whereas Ni coordination suppresses radical-quenching capacity due to stronger ligand-field stabilization and limited redox accessibility (Frenking*et al.*, 2021; Kumar*et al.*, 2023)

.

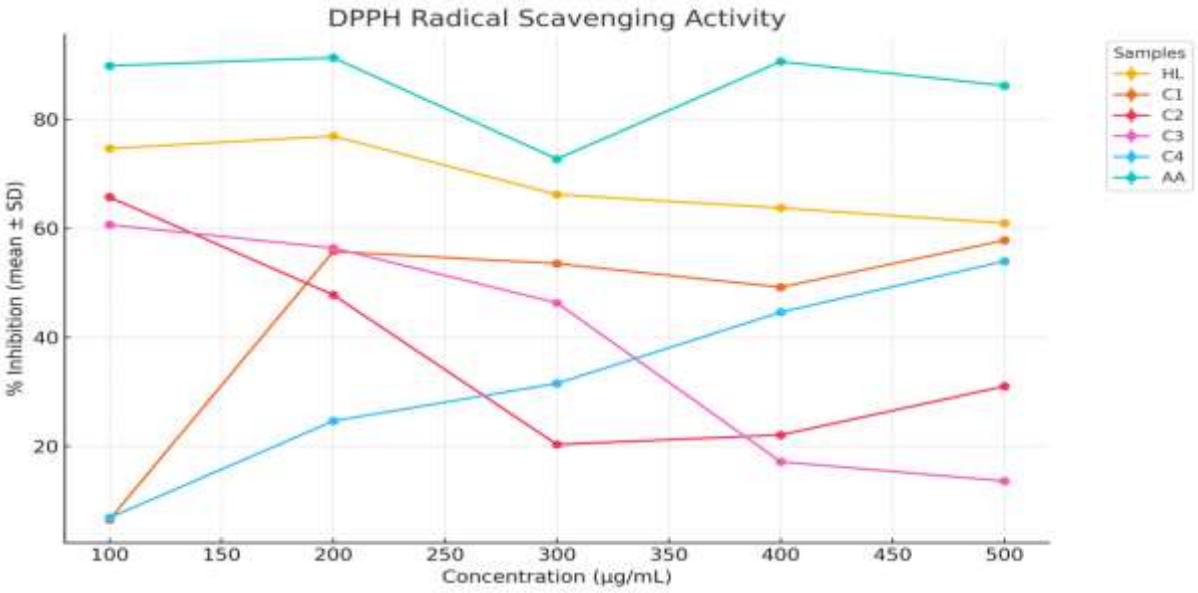

Figure 5: DPPH scavenging profiles (% inhibition, mean ± SD) for HL, C1–C4, and ascorbic acid (AA) over 100–500 µg/mL.

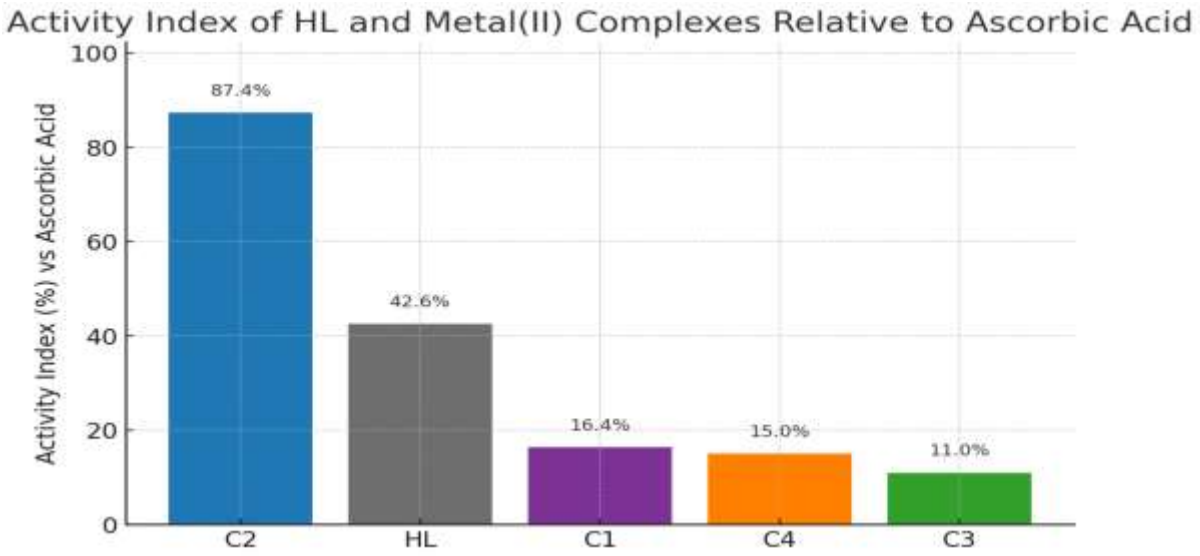

Figure 6: Activity Index (AI = sample/AA) vs concentration (AA baseline = 1).

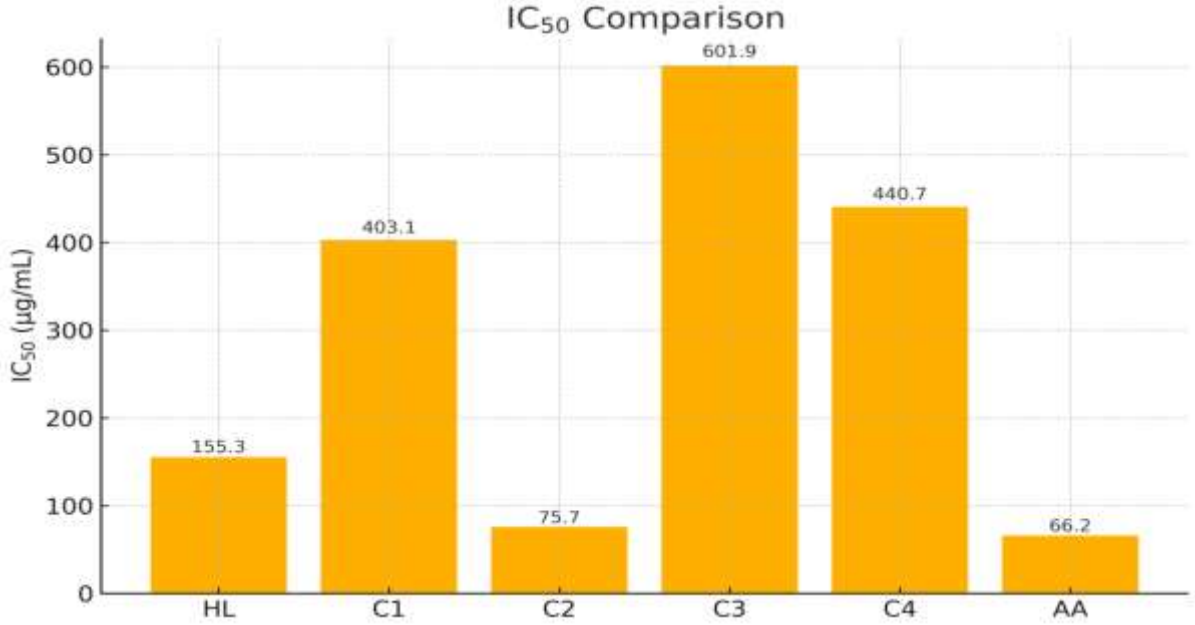

Figure 7: IC_{50} comparison (µg/mL); lower values indicate stronger activity.

Mechanism of Radical Scavenging Pathway

DPPH reduction can proceed by electron transfer (ET) and/or proton transfer. HL contains a hydroxamic motif capable of H-atom donation and ET *via* the carbonyl/N–O system, explaining its consistently high baseline activity. In metal complexes, two counteracting effects emerge: (i) Chelation control: binding delocalize the donor electron density over the –CONO– group and metal centre, which results in lowering the effective H-donation propensity (reduced and availability), and Redox mediation: certain metal ions (notably Co(II)/Cu often mediate ET through transient M/M(I) or M/M(III) couples, potentially enhancing DPPH reduction when the ligand field aligns with accessible redox states. The mechanistic illustrations presented in Figures 8 to 10 further clarify these pathways. Figure 8 depicts the three competitive routes: HAT, PCET, and ET, accessible to the free hydroxamic ligand, highlighting why HL maintains a relatively strong intrinsic radical-quenching ability. Figure 9 illustrates how complexation alters the mechanism by introducing an LMCT-assisted electron transfer pathway and possible metal-centred redox cycling, particularly favourable for Co and Cu systems. Figure 10 integrates these concepts into a structure–

activity relationship (SAR) model across the Mn–Co–Ni–Cu series, demonstrating that the balance between chelation-induced suppression of H-donation and metal-mediated ET enhancement governs the antioxidant efficiency of the complexes (Baliyan *et al.*, 2022; Gulcin & Alwasel, 2023).

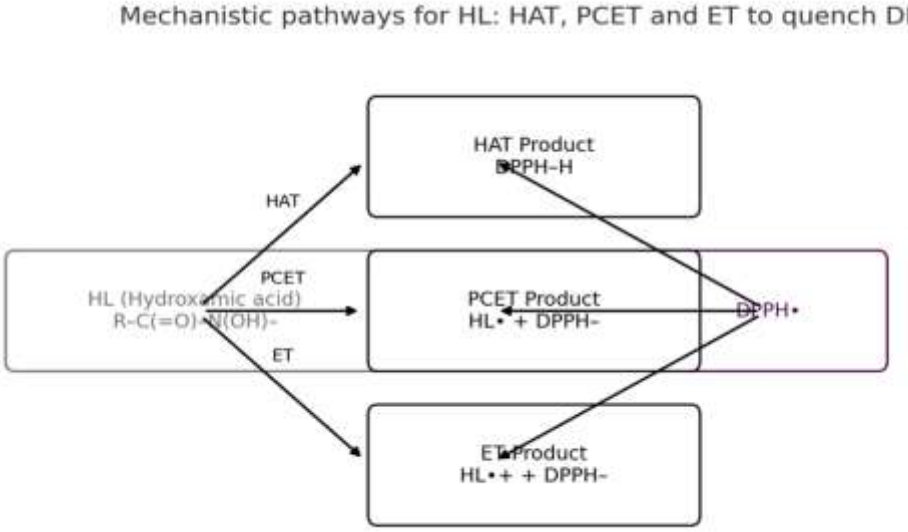

Figure 8: Balanced mechanistic routes for the free hydroxamic ligand (HL): hydrogen-atom transfer (HAT), proton-coupled electron transfer (PCET), and direct electron transfer (ET) pathways for quenching DPPH•, showing generic hydroxamate core (R–C(=O)–N(OH)–).

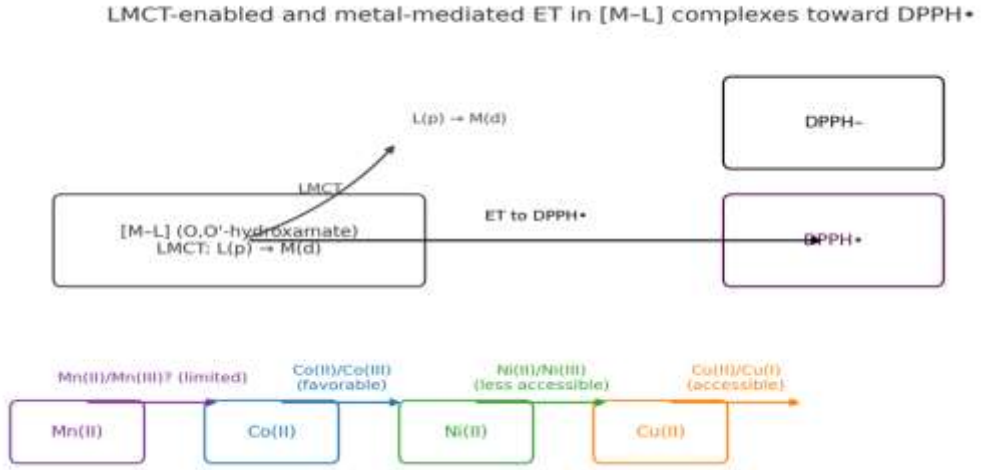

Figure 9: Schematic of ligand-to-metal charge transfer (LMCT, L(p)→M(d)) and subsequent metal-mediated electron transfer to DPPH• in O,O′-hydroxamate complexes [M–L]. Metal-specific redox accessibility is indicated: Mn/Mn(III) (limited), Co/Co(III) (favourable), Ni/Ni(III) (less accessible), and Cu/Cu(I) (accessible).

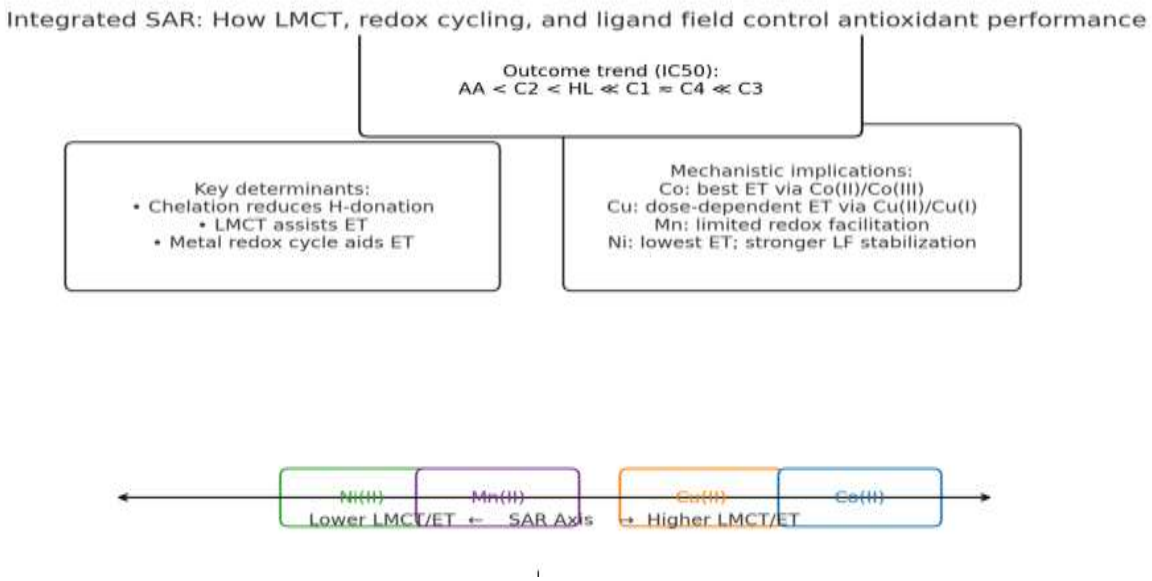

Figure 10: Integrated structure–activity map rationalizing the antioxidant trend (IC_{50}): AA < C2 < HL ≪ C1 ≈ C4 ≪ C3. The SAR axis reflects increasing LMCT/ET efficiency and redox accessibility; Co performs best *via* Co/Co(III) cycling, Cu improves with dose via Cu/Cu(I), Mn shows limited redox facilitation, and Ni displays the lowest ET propensity due to stronger ligand-field stabilization.

Structural Activity Relation (SAR)

The structure–activity relationship (SAR) of the hydroxamic acid ligand and its metal complexes can be rationalized by considering ligand electronics, metal–ligand bonding, and redox-mediated scavenging pathways governed by ligand field and HSAB principles. The free ligand (HL) displays strong antioxidant activity primarily due to its hydroxamic group, which facilitates both proton-coupled electron transfer (PCET) and direct hydrogen atom transfer (HAT) through the conjugated C=O–N–OH system. Coordination to metal ions reduces the electron density on the oxygen and nitrogen donor atoms, diminishing the intrinsic H-donating ability of the ligand; this chelation-induced suppression aligns with Tweedy's theory, although the extent of reduction depends on the metal's hardness and ligand field stabilization. From an HSAB perspective, the hard O,O-donating hydroxamate ligand binds more strongly to borderline/hard metal ions (Co^{2+}, Ni^{2+}, Mn^{2+}) than to the softer Cu^{2+}, influencing metal–ligand covalency and electron distribution. The superior performance of the Co complex (C2) arises from favourable ligand-to-metal charge transfer (LMCT) and accessible Co^{2+}/Co^{3+} redox cycling that enhances electron-transfer to DPPH. In contrast, the Ni complex (C3) exhibits the lowest activity, consistent with a more stable ligand field and limited Ni^{2+}/Ni^{3+} redox participation, which reduces LMCT contributions and locks electron density within the coordination sphere. The Cu complex (C4) shows dose-dependent enhancement linked to Cu^{2+}/Cu^{+} cycling and partial covalency of Cu–O bonds that facilitates ET at higher concentrations, while the Mn complex (C1) shows irregular activity reflective of high-spin Mn^{2+}, where ligand field stabilization is minimal and redox transitions are less favourable. Collectively, the SAR trend (Co > Cu ≥ Mn > Ni) demonstrates that antioxidant behaviour is governed by the interplay between (i) chelation-driven modulation of ligand electron donation, LMCT efficiency, (iii) metal-centred redox cycling, and (iv) ligand field effects dictating the ease of electron mobility within the coordination sphere. These findings highlight that optimal radical-scavenging performance in hydroxamate metal complexes requires not only a redox-active metal centre but also a ligand field environment that promotes LMCT-assisted electron transfer without excessively stabilizing the M–L bond (Thakur*et al.*, 2024; Venkatesh *et al.*, 2024).

CONCLUSION

A hydroxamic acid ligand (HL) was successfully synthesized and coordinated to Mn, Co, Ni, and Cu ions to afford a new series

of metal complexes (C1-C4), respectively. Structural elucidation through FTIR, UV–Vis, elemental analysis, melting point, and conductivity measurements confirmed that HL functions as a bidentate monoanionic ligand, coordinating *via* the carbonyl and deprotonated hydroxyl oxygen atoms to resulting in neutral square planar (Ni(II) and Cu(II)) and tetrahedral (Mn(II) and Co(II) complexes of the type $[M(L)_2]$. The observed spectral shifts, notably the lowering of ν(C=O) and disappearance of ν(O–H), alongside the appearance of M–O bands, provided evidence of successful chelation, while the close agreement between calculated and experimental CHN values verified the proposed stoichiometries. The antioxidant studies revealed a clear modulation of the radical scavenging activity upon metal coordination. The Co complex, exhibited the most pronounced enhancement, demonstrating activity closest to the standard ascorbic acid, while HL retained moderate efficacy. In contrast, Mn, Cu, and Ni complexes showed comparatively lower activity, suggesting that ligand–metal electronic interplay and redox accessibility strongly influence the antioxidant response. These findings underscore the relevance of ligand field effects, LMCT dynamics, and metal-centred redox behaviour in dictating bioactivity. This study provides valuable insight into the structure–activity relationships of hydroxamic acid metal complexes and establishes a platform for further biological, mechanistic, and computational investigations to expand their potential applications.

Authors Contributory Statements

All authors contributed substantially to the conception, design, and execution of the research work. Experimental synthesis, characterization studies, and data acquisition were carried out by M. S. Bute as part of her M.Sc. research project at the Department of Pure and Applied Chemistry, University of Maiduguri, Borno State, Nigeria. Data interpretation, manuscript drafting, critical review, and editing were jointly performed by all authors. All authors have read and approved the final version of the manuscript.

Conflict of Interest Statements

The authors declare that they have no known financial or personal conflicts of interest that could have influenced the work reported in this manuscript.

REFERENCES

Ali, D., & Abedullah, S. (2023). Preparation of Some Hydroxamic Acid Derivatives and Study of their Biological Activity as Anti-Cancer and Anti-Bacterial Agents. *HIV Nurs*, *23*, 809-816.

Aneja, B., Khan, P., Alam, S., Hasan, P., & Abid, M. (2020). Ferulic Hydroxamic Acid Triazole Hybrids as Peptide Deformylase Inhibitors: Synthesis, Molecular Modelling and Biological Evaluation. *ChemistrySelect*, *5*(37), 11420-11430.

Azimi, S. G., Shakour, N., Bagherzade, G., Saberi, M. R., Azimi, H., & Moosavi F, M. (2025). A Comprehensive Review of the Biological Activities of Medicinal Metal Complexes Synthesized From Quinoline Scaffolds. *Bioinorganic Chemistry and Applications*, *2025*(1), 3133615.

Bagul, A., Gaikwad, D., & Patil, Y. (2023). Synthesis and Characterization of Some Transition Complexes with 4-[2-(2-chlorobenzylidene) hydrazinyl]-7H-pyrrolo [2, 3-d] pyrimidine: Antimicrobial and Cytotoxic Activity.

Baliyan, S., Mukherjee, R., Priyadarshini, A., Vibhuti, A., Gupta, A., Pandey, R. P., & Chang, C.-M. (2022). Determination of antioxidants by DPPH radical scavenging activity and quantitative phytochemical analysis of Ficus religiosa. *Molecules*, *27*(4), 1326.

Citarella, A., Moi, D., Pinzi, L., Bonanni, D., & Rastelli, G. (2021). Hydroxamic acid derivatives: From synthetic strategies to medicinal chemistry applications. *ACS omega*, *6*(34), 21843-21849.

de Araújo Queirós, C. P. (2018). *Fluorescent ligands and coordination polymers with potential application in metal ion sensing, photoluminescence and heterogeneous catalysis* Universidade do Porto (Portugal)].

Frenking, G., Fernández, I., Holzmann, N., Pan, S., Krossing, I., & Zhou, M. (2021). Metal–CO bonding in mononuclear transition metal carbonyl complexes. *Jacs Au*, *1*(5), 623-645.

Fugu, M. B., Coley, J., Dickinson, I. F., Orton, J. B., Klooster, W., Gleeson, M. P., & Jones, L. F. (2021). Slight ligand

modifications within multitopic linear hydroxamates promotes connectivity differences in Cu (II) 1-D coordination polymers. *crystengcomm*, *23*(32), 5531-5539.

Gambino, D., & Otero, L. (2023). Prospective metallo-drugs including bioactive compounds: selection of co-ligands to tune biological activity against neglected tropical diseases. In *Targeted Metallo-Drugs* (pp. 193-214). CRC Press.

Gani, R. S., Kudva, A. K., Timanagouda, K., Mujawar, S. B. H., Joshi, S. D., & Raghu, S. V. (2021). Synthesis of novel 5-(2, 5-bis (2, 2, 2-trifluoroethoxy) phenyl)-1, 3, 4-oxadiazole-2-thiol derivatives as potential glucosidase inhibitors. *Bioorganic Chemistry*, *114*, 105046.

Gulcin, İ., & Alwasel, S. H. (2023). DPPH radical scavenging assay. *Processes*, *11*(8), 2248.

Hao, H. (2020). *Titanium-catalyzed hydroamination: mechanism, reactivity and applications* University of British Columbia].

Hassan, L. R., Ramasamy, K., Lim, S. M., Bahron, H., & Tajuddin, A. M. (2018). Synthesis and characterization of benzohydroxamic acid metal complexes and their cytotoxicity study. *Jurnal Teknologi (Sciences & Engineering)*, *80*(6).

He, M. (2019). *Complexation of actinides and analogues with hydroxamate ligands* Université Paris-Saclay].

Healy, C., Patil, K. M., Wilson, B. H., Hermanspahn, L., Harvey-Reid, N. C., Howard, B. I., Kleinjan, C., Kolien, J., Payet, F., & Telfer, S. G. (2020). The thermal stability of metal-organic frameworks. *Coordination Chemistry Reviews*, *419*, 213388.

Howsaui, H. B., Sharfalddin, A. A., Abdellattif, M. H., Basaleh, A. S., & Hussien, M. A. (2021). Synthesis, spectroscopic characterization and biological studies of Mn (II), Cu (Ii), Ni (II), Co (II) and Zn (II) complexes with new schiff base of 2-((pyrazine-2-ylimino) methyl) phenol. *Applied Sciences*, *11*(19), 9067.

Keth, J., Johann, T., & Frey, H. (2020). Hydroxamic acid: An underrated moiety? marrying bioinorganic chemistry and polymer science. *Biomacromolecules*, *21*(7), 2546-2556.

Korkmaz, I. N., & Özdemir, H. (2022). Synthesis and anticancer potential of new hydroxamic acid derivatives as chemotherapeutic agents. *Applied Biochemistry and Biotechnology*, *194*(12), 6349-6366.

Kothawade, S., & Shende, P. (2024). Coordination bonded stimuli-responsive drug delivery system of chemical actives with metal in pharmaceutical applications. *Coordination Chemistry Reviews*, *510*, 215851.

Kumar, M., Singh, A. K., Singh, V. K., Yadav, R. K., Singh, A. P., & Singh, S. (2024). Recent developments in the biological activities of 3d-metal complexes with salicylaldehyde-based N, O-donor Schiff base ligands. *Coordination Chemistry Reviews*, *505*, 215663.

Kumar, N., Kaushal, R., & Awasthi, P. (2023). Non-covalent binding studies of transition metal complexes with DNA: A review. *Journal of Molecular Structure*, *1288*, 135751.

Mohammed, B. F. (2019). *Novel di-and multitopic hydroxamate ligands towards discrete and extended network complexes*. Bangor University (United Kingdom).

Naeem, M., Ashraf, A., Imran, M., Siddiqui, W. A., Muhammad, G., Saleem, A., Younas, U., Ali, F., Raza, M. A., & Mitu, L. (2025). Oxicams as Bioactive Ligand System in Coordination Complexes and Their Biological Applications. *Comments on Inorganic Chemistry*, *45*(2), 63-87.

Pooja, G., Shweta, S., & Patel, P. (2025). Oxidative stress and free radicals in disease pathogenesis: a review. *Discover Medicine*, *2*(1), 104.

Rahban, M., Zolghadri, S., Salehi, N., Ahmad, F., Haertlé, T., Rezaei-Ghaleh, N., Sawyer, L., & Saboury, A. A. (2022). Thermal stability enhancement: Fundamental concepts of protein engineering strategies to manipulate the flexible structure. *International*

journal of biological macromolecules, *214*, 642-654.

Reddy, V. P. (2023). Oxidative stress in health and disease. *Biomedicines*, *11*(11), 2925.

Sadiq, I. Z. (2023). Free radicals and oxidative stress: Signaling mechanisms, redox basis for human diseases, and cell cycle regulation. *Current molecular medicine*, *23*(1), 13-35.

Saleem, F., Khan, N., & Ali, I. (2020). Synthesis of hydroxamic ligands with transition metal complexes, their biological activities and characterization through spectroscopic techniques. *Al-Nahrain Journal of Science*, *23*(2), 1-7.

Sow, I. S., Gelbcke, M., Meyer, F., Vandeput, M., Marloye, M., Basov, S., Van Bael, M. J., Berger, G., Robeyns, K., & Hermans, S. (2023). Synthesis and biological activity of iron (II), iron (III), nickel (II), copper (II) and zinc (II) complexes of aliphatic hydroxamic acids. *Journal of Coordination Chemistry*, *76*(1), 76-105.

Syed, Z., Sonu, K., Dongre, A., Sharma, G., & Sogani, M. (2020). A review on hydroxamic acids: Widespectrum chemotherapeutic agents. *Int. J. Biol. Biomed. Eng*, *14*, 75-88.

Thakur, S., Jaryal, A., & Bhalla, A. (2024). Recent advances in biological and medicinal profile of Schiff bases and their metal complexes: an updated version (2018–2023). Results Chem 7: 101350. In.

Venkatesh, G., Vennila, P., Kaya, S., Ahmed, S. B., Sumathi, P., Siva, V., Rajendran, P., & Kamal, C. (2024). Synthesis and spectroscopic characterization of Schiff base metal complexes, biological activity, and molecular docking studies. *ACS omega*, *9*(7), 8123-8138.

Waziri, I., Mala, G. A., Wakil, I. M., Coetzee, L.-C. C., & Garba, H. (2023). Template Synthesis of Ni (II) and Zn (II) Complexes Derived from N2O2 Donor Symmetrical Tetradentate Ligands System: Comparative Antioxidant, Xanthine inhibitory, and Computational Studies. *Ar. ZJ Bas. Appl. Res.*, *2*(1), 30-58.

Waziri, I., Yusuf, T. L., Zarma, H. A., Oselusi, S. O., Coetzee, L.-C. C., & Adeyinka, A. S. (2023). New palladium (II) complexes from halogen substituted Schiff base ligands: Synthesis, spectroscopic, biological activity, density functional theory, and molecular docking investigations. *Inorganica Chimica Acta*, *552*, 121505.